

## Determining the Impact of Dynamic Load Conditions on Interfacial Liquid Water Accumulation in Polymer Electrolyte Membrane Fuel Cell Gas Diffusion Layers Using Synchrotron X-Ray Radiography

R. Banerjee, N. Ge, J. Lee, M.G. George, H. Liu, D. Muirhead, P. Shrestha, S. Chevalier, J. Hinebaugh and A. Bazylak

Thermofluids for Energy and Advanced Materials (TEAM) Laboratory  
Department of Mechanical and Industrial Engineering,  
University of Toronto Institute for Sustainable Energy  
Faculty of Applied Science and Engineering,  
University of Toronto, Toronto Ontario, Canada

Automotive power demand is dynamic, so the transient multiphase transport behavior must be understood and considered in the design of next generation polymer electrolyte membrane (PEM) fuel cell materials. In-operando synchrotron X-ray radiography was used to measure the changes in liquid water saturation of the gas diffusion layer (GDL) during changes in operational current density. Through in-operando visualizations at high temporal and spatial resolutions, we observed that the liquid water saturation of the GDL increases with increasing current density, but a threshold saturation in the GDL is eventually reached, despite further increases in current density. A time lag between the change in current density and the onset of increasing GDL saturation was also observed.

### Introduction

The polymer electrolyte membrane (PEM) fuel cell has been identified as the most prominent candidate for replacing the internal combustion engine by major automakers around the world and the US Department of Energy (US-DOE) (1). Water transport through the PEM fuel cell is one of the most influential factors to operational performance (2 – 6). Under automotive conditions, the power demand varies continuously (7 – 11). Therefore, it is important to understand the extent to which dynamic behaviour should be considered during transient conditions. Banerjee and Kandlikar (7) provided a comprehensive review of various transient responses observed during PEM fuel cell operation. The liquid water saturation in the gas diffusion layer (GDL) is one parameter that requires significant time to reach steady state. With the advent of several fuel cell powertrain vehicles from automakers, it is important to understand the operational considerations and therefore include the transient time scales into current fuel cell models. Understanding how the operating conditions impact transient time scales will enable improved real time predictions of performance and operational requirements.

One of the key functions of the GDL is to effectively distribute the reactant gases from the reactant channels to the catalytic reaction sites. Detailed reviews of the GDL have been provided by Cindrella et al. (12) and Park et al. (13). These reviews provide a rich overview of GDL materials, designs and characterization methods. The GDL has a high porosity

(typically above 70%) in order to facilitate pathways for reactant gas transport (14). However, if liquid water accumulates in the pores of the GDL, the number of available gaseous transport pathways decreases, thereby increasing the mass transport resistance. The effective porosity available for gaseous transport therefore decreases with increases in liquid water saturation of the GDL. Owejan et al. (15) observed increases in oxygen transport resistance with increasing water saturation of the GDL.

Banerjee and Kandlikar (16) showed that changes in temperature and operating load result in long transient times for the pressure drop and cell voltage to reach steady state. The pressure drop was observed to be a direct indicator of liquid water in the channels and an indirect indicator of the GDL saturation (17). Banerjee and Kandlikar (18) also observed that significant times were required for the pressure drop in the gas channels to reach steady state. This was hypothesized to be related to the change in water removal rates from the GDL due to changing gas velocities in the channel. A direct visualization of the GDL saturation would aid the understanding of transient water removal from the GDL.

Manke et al. (19) used synchrotron X-ray radiography to visualize the evolution of water droplets into the channel and showed that water emergence was a periodic phenomenon. Boillat et al. (20) used neutron imaging to show that the water saturation in the GDL requires up to ten minutes to stabilize in response to a change in inlet relative humidity conditions. Deevanhxay et al. (21) used soft X-ray radiography to investigate the through-plane water thickness profiles. They found that at low current densities of up to  $0.6 \text{ A/cm}^2$ , 150 seconds were required for the water profiles to stabilize after a change in current density.

The liquid water saturation of the GDL also changes with time, even with all other operating parameters held constant. Wang and Wang (22) used a numerical model to study the impact of change in the inlet humidification of the cathode. They demonstrated that 25 seconds were necessary for the GDL saturation to change due to a change in inlet humidification. Song et al. (23) also developed a non-isothermal model to study the transient changes in liquid water saturation. They showed that the transient nature of liquid water saturation in the GDL is also a function of the absolute water saturation at the start of the change. They also showed that the transient behaviour reached steady state at a much faster rate at higher current densities due to higher rates of water production.

Most studies involving transient investigations of GDL saturation have been explored in the numerical domain (22 – 25), with a scarcity of experimental literature available for validation. These results can be validated and further explored using the technique of synchrotron X-ray radiography, which provides the ability to visualize the changes in liquid water saturation in the GDL with high spatial and temporal resolutions. In the present work, the transient changes in GDL water saturation were measured during in-operando synchrotron X-ray radiographic visualizations. The operating current density was changed during the experiment and the temporal behavior of liquid water saturation in the GDL was monitored until steady state liquid water saturation was reached. Additionally, the local distribution of the water was also investigated to identify the time required for the steady state to be achieved.

## Methodology

### Experimental Methodology

A custom-built miniature fuel cell was designed for optimal imaging conditions at the Canadian Light Source Inc. BMIT-BM (05B1-1) beamline (26). The cell had an active area of  $0.68 \text{ cm}^2$  and a Nafion HP membrane from IonPower<sup>®</sup> with  $0.3 \text{ mg/cm}^2$  Pt/C loading on both sides of the membrane was used. Two fuel cell builds were used to study the transient behaviour of liquid water saturation. An SGL 25BC GDL was used in the first build, while an SGL 29BC GDL was used in the second build. The MEA was housed between graphite flow field plates, which had  $0.5 \text{ mm}$ -thick channel and land regions, resulting in a periodic width of  $1.0 \text{ mm}$ .

For all the tests described in this study, the anode and cathode flow rates were maintained at constant gas flow rates of  $1.0 \text{ liters/min}$ . These flow rates resulted in high stoichiometric ratios that were intentionally chosen to establish quasi one-dimensional transport behaviour, whereby the GDL saturation would not be dominated by water accumulation in the gas channels. An operating temperature of  $60^\circ\text{C}$  and fully humidified inlet gases were maintained during the entire study. The intentionally high relative humidity conditions accelerated the accumulation of liquid water within the GDL. The temperature used here enables a direct comparison to the behaviour discussed by Banerjee and Kandlikar (16,18).

The water generation is expected to change with current density, while all other transport related parameters such as gas flow rates, evaporation rates, and water removal rates will remain constant. Therefore, during the periods of constant gas flow rates, the liquid water saturation of the GDL gradually approached a steady state value for the specific current density of operation. This transient behaviour of liquid water accumulation in the GDL is the focus of this study.

### Radiography

The experiments were carried out at the Biomedical Imaging and Therapy – Bending Magnet (0505B1-1) beamline at the Canadian Light Source Inc. (CLSi) in Saskatoon, Canada (26). The radiography was conducted at an energy level of  $24 \text{ keV}$ . Images were captured using an A40 scintillator and a C11440-22CU Hamamatsu CCD camera. The images obtained provided a  $6.5 \mu\text{m}/\text{pixel}$  resolution and were recorded at a frame rate of  $0.33 \text{ frames per second (fps)}$ . Figure 1 provides a schematic of the fuel cell imaging setup used in this study.

Dry state (reference) images were obtained at open circuit voltage (OCV) to compare with the wet state (test) images obtained during fuel cell operation. The water thickness in the GDL was obtained by processing the wet state images with an algorithm developed in-house. The dry state images and the test case (wet) images were used in the Beer Lambert law to quantify the liquid water present in the GDL. The details of the image processing algorithm are presented in detail by Hinebaugh et al. (27) and Ge et al. (28).

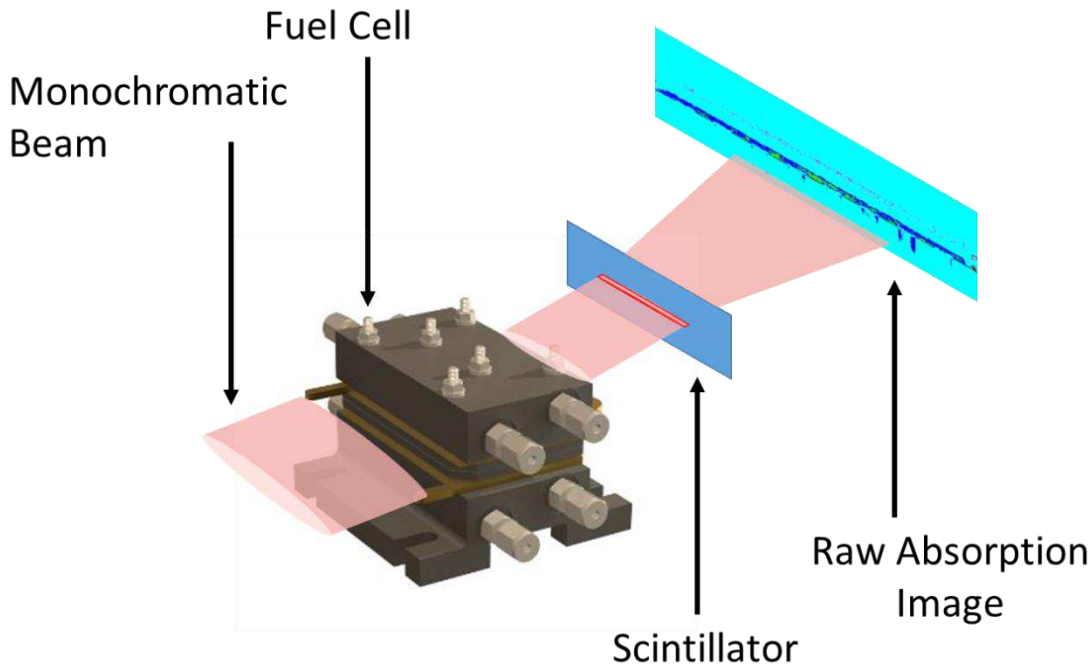


Figure 1. Schematic of fuel cell imaging setup.

#### Data Processing

Radiographic images that elucidate the dynamic liquid water transport within the fuel cell were concurrently obtained with performance measurements. Radiographic image stacks were obtained from the CCD camera. A custom image processing algorithm developed in-house (27, 28) was applied to quantify the liquid water present throughout the experiments. The liquid water in the fuel cell was quantified, and the spatial distribution of liquid water was determined in such a way that water in the MPL, carbon paper substrate, and gas flow fields was distinct. For each stack of images (representing a single experiment), a region of interest was selected in the carbon paper that encompassed eight gas flow channels and seven land regions. The liquid water content in this region of interest was averaged and presented as a function of time, and this liquid water content was directly correlated to the real-time operating conditions of the fuel cell.

#### Results

The current density was increased in a shallow step-wise fashion from zero current by  $0.5 \text{ A/cm}^2$  with a ramp (at a rate of  $0.001 \text{ A/s}$ ), until high current densities were reached. The fully humidified reactant gas flow rate was held at a constant value throughout; therefore, changes in water removal rates via advection were not expected. These conditions led to measurable changes in the liquid water thickness in the GDL.

Figure 2 shows the changes in normalized liquid water thickness in the GDL for SGL 25BC along with the corresponding step changes in applied current density and voltage responses from the cell. The water thickness as obtained from the radiographs are normalized by the length of GDL in the beam path, i.e. 8 mm of GDL. This makes the normalized liquid water thickness usable for any other system, where the conditions are

known. The current density was sequentially increased from zero current in five consecutive constant current density steps, where steady state was achieved by holding each operational point for 15 minutes. The normalized water thickness in the GDL was determined from the radiographic images described in the previous section. The mean of the GDL section (consisting of eight channels and seven land regions) has been reported.

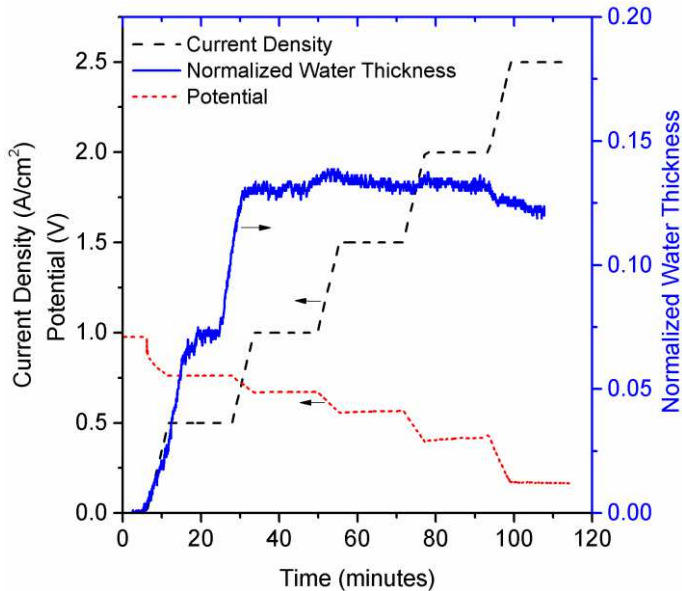


Figure 2. Normalized water thickness (SGL 25BC) as a function of time, corresponding to the change in current density.

It can be observed that at lower current densities, with an increase in the operating current density, the normalized water thickness also increases. This is expected because it was assumed that the rate of water vapour removal remained constant since constant reactant gas flow rates were used. Therefore, upon increasing the operating current density (and the associated water generation rate) with a constant water vapour removal rate, a new equilibrium in liquid water thickness in the GDL was reached. The new equilibrium facilitated greater quantities of liquid water to exit the GDL via established breakthrough pathways, while a consistent quantity of water remained in the GDL pores. However, this behaviour is observed only for the first two increases in current density, i.e. from zero current to  $0.5\text{ A}/\text{cm}^2$  and then from  $0.5\text{ A}/\text{cm}^2$  to  $1.0\text{ A}/\text{cm}^2$ . Once the normalized liquid water thickness reached a value over 0.13 (at a current density of  $1.0\text{ A}/\text{cm}^2$ ), no further increases in water thickness were observed with increasing current density. A normalized water thickness value of 0.13 appeared to be a threshold water thickness value.

Figure 3 shows changes in normalized liquid water thicknesses for SGL 29BC along with the cell potential and operating current density. This fuel cell reached a current density of  $2.0\text{ A}/\text{cm}^2$  with the same changes in current density as in the case of SGL 25BC. An increased number of fluctuations were observed in the normalized water thicknesses compared to the case with SGL 25BC. During the first current density increase, from zero current to  $0.5\text{ A}/\text{cm}^2$ , the normalized water thickness increased with the increase in current density. Even though the current density was held constant for 15 minutes at  $0.5\text{ A}/\text{cm}^2$ , the water saturation continued to increase throughout the 15 minutes without reaching a steady state value. When the next change in current density was applied ( $1.0\text{ A}/\text{cm}^2$ ), the water thickness increased without a delayed response. The steady water thickness reached

a value of 0.15, similar to that for SGL 25BC. This upper plateau did not change with further increases in current density.

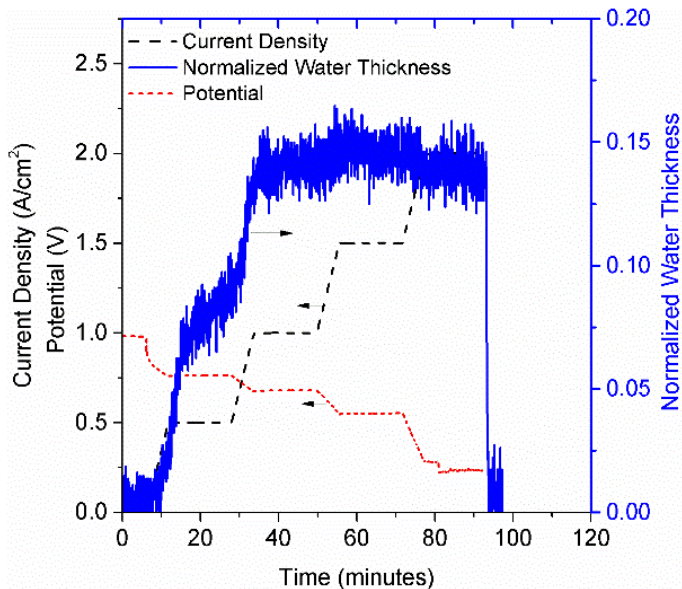


Figure 3. Normalized water thickness (SGL 29BC) as a function of time, corresponding to the change in current density.

Figure 4 shows the dynamic response of water thickness during the first change in current density for the cell build with SGL 25BC (shown in Figure 2). The current density was increased from zero current to  $0.5 \text{ A}/\text{cm}^2$  in a ramped increase over a period of 5.6 minutes. Although the water content increased with increasing current density, the water quantity did not reach a steady state value even after the current density stabilized after 5.6 minutes. The measured water thickness continued to increase for several minutes before reaching a steady state value. This continued change in measured water thickness indicated a change in saturation of the GDL, which results in an increased reactant transport resistance and therefore reduced performance. Several factors may influence the time required to reach steady saturation, such as ramp rates of changing current density and the gas flow rates in the channels.

The information coming from these experiments can be used to inform transient models which can predict the change in saturation levels within the GDL. As observed here the average normalized water thickness does not go beyond an upper threshold which lies at approximately 0.13. This will also inform the volume of water expected to accumulate within the GDL pores.

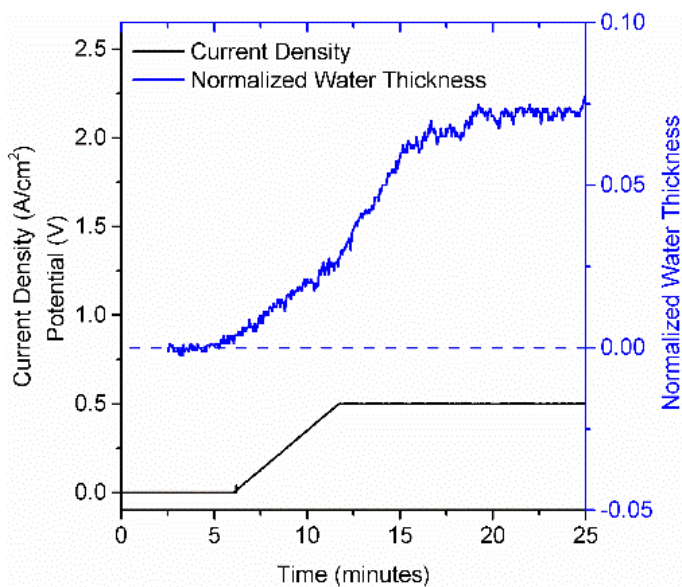


Figure 4. Zoomed in visualization of change in normalized liquid water with change in current density for SGL 25BC. The lag in time between when the current density reaches a steady state and the normalized water reaches a steady state is shown.

## Conclusions

In this work, the temporal change in liquid water saturation within the gas diffusion layer of PEM fuel cells was investigated. In-operando X-ray radiography was performed on a custom-built fuel cell, specifically designed to have a small X-ray footprint. Changes in current density were implemented in order to observe the impact of changing water generation rates on water saturation in the GDL with high temporal resolution. The following key findings were obtained from this study:

- An upper threshold exists for the liquid water content in the GDL, whereby further increases in current density do not impact the liquid water content.
- A time lag was observed between increasing the operating load and observing changes to the GDL liquid water content.
- Although the change in current density occurred over a period of 150 seconds (2.5 minutes), in several cases the local water content did not reach a steady state value even after significant period of time (15 minutes).

The work presented here shows that concurrently monitoring the performance and the transient liquid water accumulation in the fuel cell provides a valuable technique for evaluating design factors (involving material properties and operating conditions), which significantly impact the GDL liquid water saturation.

## Acknowledgements

Financial support from the Natural Sciences and Engineering Research Council of Canada (NSERC), the NSERC Discovery Accelerator Program, the NSERC Canada

Research Chairs Program, the Ontario Ministry of Research and Innovation Early Researcher Award, and the Canada Foundation for Innovation are gratefully acknowledged.

Research described in this paper was performed at the BMIT facility at the Canadian Light Source, which is funded by the Canada Foundation for Innovation, the Natural Sciences and Engineering Research Council of Canada, the National Research Council Canada, the Canadian Institutes of Health Research, the Government of Saskatchewan, Western Economic Diversification Canada, and the University of Saskatchewan. Authors acknowledge the receipt of support from the CLS Post-Doctoral and Graduate Student Travel Support Program.

## References

1. P. Costamagna and S. Srinivasan, *J. Power Sources*, **102**, 242–252 (2001).
2. S. G. Kandlikar, *Heat Transfer Eng.*, **29**, 575–587 (2008).
3. S. G. Kandlikar and Z. Lu, *J. Fuel Cell Sci. Technol.*, **6**, 44001 (2009).
4. Quick, C., Ritzinger, D., Lehnert, W., and Hartnig, C., *J. Power Sources*, **190**, 110–120 (2009).
5. J. P. Owejan, J. J. Gagliardo, J. M. Sergi, S. G. Kandlikar, and T. A. Trabold, *Int. J. Hydrogen Energy*, **34**, 3436–3444 (2009).
6. S. G. Kandlikar, E. J. See, M. Koz, P. Gopalan, and R. Banerjee, *Int. J. Hydrogen Energy*, **39**, 6620–6636 (2014).
7. R. Banerjee and S. G. Kandlikar, *Int. J. Hydrogen Energy*, **40**, 3990–4010 (2015).
8. A. F. Pacheco, M. E. S. Martins, and H. Zhao, *Fuel*, **111**, 733–739 (2013).
9. S. F. Tie and C. W. Tan, *Renew. Sustain. Energy Rev.*, **20**, 82–102 (2013).
10. P. Corbo, F. E. Corcione, F. Migliardini, and O. Veneri, *J. Power Sources*, **145**, 610–619 (2005).
11. D. D. Boettner, G. Paganelli, Y. G. Guezennec, G. Rizzoni, and M. J. Moran, *J. Energy Resour. Technol.*, **124**, 20–27 (2002).
12. L. Cindrella, A.M. Kannan, J.F. Lin, K. Saminathan, Y. Ho, C.W. Lin, J. Wertz, *J. Power Sources*, **194**, 146–160 (2009).
13. S. Park, J.-W. Lee, and B. N. Popov, *Int. J. Hydrogen Energy*, **37**, 5850–5865 (2012).
14. R. Banerjee, J. Hinebaugh, H. Liu, R. Yip, N. Ge, and A. Bazylak, *Int. J. Hydrogen Energy* (2016).
15. J. P. Owejan, T. A. Trabold, and M. M. Mench, *Int. J. Heat Mass Transfer*, **71**, 585–592 (2014).
16. R. Banerjee and S. G. Kandlikar, *J. Power Sources*, **268**, 194–203 (2014).
17. R. Banerjee, D. Howe, V. Mejia, and S. G. Kandlikar, *Int. J. Hydrogen Energy*, **39**, 17791–17801 (2014).
18. R. Banerjee and S. G. Kandlikar, *Int. J. Hydrogen Energy*, **39**, 19079–19086 (2014).
19. I. Manke, C. Hartnig, M. Grünerbel, W. Lehnert, N. Kardjilov, A. Haibel, A. Hilger, J. Banhart, and H. Riesemeier, *Appl. Phys. Lett.*, **90**, 174105-174105-3 (2007).
20. P. Boillat, P. Oberholzer, A. Kaestner, R. Siegrist, E.H. Lehmann, G.G. Scherer, A. Wokaun, *J. Electrochem. Soc.*, **159**, F210–F218 (2012).
21. P. Deevanhxay, T. Sasabe, S. Tsushima, and S. Hirai, *J. Power Sources*, **230**, 38–43 (2013).

22. Y. Wang and C.-Y. Wang, *Electrochimica Acta*, **50**, 1307–1315 (2005).
23. D. Song, Q. Wang, Z.-S. Liu, and C. Huang, *J. Power Sources*, **159**, 928–942 (2006).
24. D. Natarajan and T. Van Nguyen, *J. Electrochem. Soc.*, **148**, A1324–A1335 (2001).
25. Y. Wang and C.-Y. Wang, *J. Electrochem. Soc.*, **154**, B636 (2007).
26. T. W. Wysokinski, D. Chapman, G. Adams, M. Renier, P. Suortti, and W. Thomlinson, *Nucl. Instrum. Methods Phys. Res. Sect. Accel. Spectrometers Detect. Assoc. Equip.*, **582**, 73–76 (2007).
27. J. Hinebaugh, P. R. Challa, and A. Bazylak, *J. Synchrotron Radiat.*, **19**, 994–1000 (2012).
28. N. Ge, S. Chevalier, J. Hinebaugh, R. Yip, J. Lee, P. Antonacci, T. Kotaka, Y. Tabuchi, and A. Bazylak, *J. Synchrotron Radiat.*, **23**, 590–599 (2016).